



Partial aperture imaging by systems with annular phase coded masks

ANGIKA BULBUL,^{1,2,*} A. VIJAYAKUMAR,^{1,2} AND JOSEPH ROSEN¹

¹Department of Electrical and Computer Engineering, Ben-Gurion University of the Negev, P.O. Box 653, Beer-Sheva 8410501, Israel

²The authors contributed equally to the work

*angikabulbul@gmail.com

Abstract: Interferenceless coded aperture correlation holography is a recently developed technique for indirect 3D imaging of objects without two-wave interference. In such systems, the intensity response to a point is first recorded by modulating the light diffracted from a point object by a pseudorandom coded phase mask (CPM). The object intensity response is recorded under identical conditions and with the same CPM by mounting an object at the same axial location as of the point object. The image of the object is reconstructed by a cross-correlation between the above two responses. In the present study, the imaging capabilities of a system with partial apertures are demonstrated by synthesizing the CPM in the shape of a ring. The partial aperture system demonstrates 3D imaging capabilities with an area as low as 1.4% of the total aperture area, which is beyond the limits of a regular imaging system. These superior imaging capabilities of the new technique might be useful for imaging with ground and space telescopes.

© 2017 Optical Society of America under the terms of the [OSA Open Access Publishing Agreement](#)

OCIS codes: (170.1630) Coded aperture imaging; (090.1995) Digital holography; (110.0110) Imaging systems; (050.5080) Phase shift; (050.0050) Diffraction and gratings.

References and links

1. O. Darrigol, *A History of Optics from Greek Antiquity to the Nineteenth Century* (OUP Oxford, 2012).
2. G. S. Spagnolo and D. Ambrosini, "Successful pinhole photography," *Am. J. Phys.* **65**(3), 256–257 (1997).
3. J. C. Marron and K. S. Schroeder, "Three-dimensional lensless imaging using laser frequency diversity," *Appl. Opt.* **31**(2), 255–262 (1992).
4. A. Greenbaum, W. Luo, T.-W. Su, Z. Göröcs, L. Xue, S. O. Isikman, A. F. Coskun, O. Mudanyali, and A. Ozcan, "Imaging without lenses: achievements and remaining challenges of wide-field on-chip microscopy," *Nat. Methods* **9**(9), 889–895 (2012).
5. J. Cheng, "Ghost imaging through turbulent atmosphere," *Opt. Express* **17**(10), 7916–7921 (2009).
6. H. B. Edwards, "Lensless scanning telescope," *Appl. Opt.* **19**(4), 504–507 (1980).
7. R. A. Hyde, "Eyeglass. 1. Very large aperture diffractive telescopes," *Appl. Opt.* **38**(19), 4198–4212 (1999).
8. J. E. Harvey and C. Ftaclas, "Field-of-view limitations of phased telescope arrays," *Appl. Opt.* **34**(25), 5787–5798 (1995).
9. J. E. Harvey, A. B. Wissinger, and A. N. Bunner, "A parametric study of various synthetic aperture telescope configurations for coherent imaging applications," in *Infrared, Adaptive, and Synthetic Aperture Optical Systems*, J. S. Fender, R. B. Johnson, W. L. Wolfe, eds., *Proc. Soc. Photo-Opt. Instrum. Eng.* **643**, 194–207 (1986).
10. A. A. Michelson, "On the application of interference methods to astronomical measurements," *Proc. Natl. Acad. Sci. U.S.A.* **6**(8), 474–475 (1920).
11. R. Okayasu, M. Inoue, N. Kawaguchi, S. Kameno, K. Shibata, and Y. Asaki, "Space VLBI spacecraft HALCA and its engineering accomplishments," *Acta Astronaut.* **50**(5), 301–309 (2002).
12. Y. Kashter, Y. Rivenson, A. Stern, and J. Rosen, "Sparse synthetic aperture with Fresnel elements (S-SAFE) using digital incoherent holograms," *Opt. Express* **23**(16), 20941–20960 (2015).
13. B. Katz and J. Rosen, "Could SAFE concept be applied for designing a new synthetic aperture telescope?" *Opt. Express* **19**(6), 4924–4936 (2011).
14. J. Rosen and G. Brooker, "Digital spatially incoherent Fresnel holography," *Opt. Lett.* **32**(8), 912–914 (2007).
15. J. Rosen, N. Siegel, and G. Brooker, "Theoretical and experimental demonstration of resolution beyond the Rayleigh limit by FINCH fluorescence microscopic imaging," *Opt. Express* **19**(27), 26249–26268 (2011).
16. A. Vijayakumar, Y. Kashter, R. Kelner, and J. Rosen, "Coded aperture correlation holography—a new type of incoherent digital holograms," *Opt. Express* **24**(11), 12430–12441 (2016).

17. A. Vijayakumar and J. Rosen, "Spectrum and space resolved 4D imaging by coded aperture correlation holography (COACH) with diffractive objective lens," *Opt. Lett.* **42**(5), 947–950 (2017).
18. Y. Kashter, A. Vijayakumar, and J. Rosen, "Resolving images by blurring - a new superresolution method using a scattering mask between the observed objects and the hologram recorder," *Optica* **4**(8), 932–939 (2017).
19. A. Vijayakumar and J. Rosen, "Interferenceless coded aperture correlation holography-a new technique for recording incoherent digital holograms without two-wave interference," *Opt. Express* **25**(12), 13883–13896 (2017).
20. R. W. Gerchberg and W. O. Saxton, "A practical algorithm for the determination of phase from image and diffraction plane pictures," *Optik (Stuttg.)* **35**(2), 227–246 (1972).
21. M. Kumar, A. Vijayakumar, and J. Rosen, "Incoherent digital holograms acquired by interferenceless coded aperture correlation holography system without refractive lenses," *Sci. Rep.* **7**(1), 11555 (2017).
22. M. Ratnam Rai, A. Vijayakumar, and J. Rosen, "Single camera shot interferenceless coded aperture correlation holography," *Opt. Lett.* **42**(19), 3992–3995 (2017).
23. A. Vijayakumar, Y. Kashter, R. Kelner, and J. Rosen, "Coded aperture correlation holography system with improved performance [Invited]," *Appl. Opt.* **56**(13), F67–F77 (2017).
24. Y. N. Sulai and A. Dubra, "Adaptive optics scanning ophthalmoscopy with annular pupils," *Biomed. Opt. Express* **3**(7), 1647–1661 (2012).
25. C. J. R. Sheppard and T. Wilson, "Imaging properties of annular lenses," *Appl. Opt.* **18**(22), 3764–3769 (1979).
26. Y. Horikawa, "Resolution of annular-pupil optical systems," *J. Opt. Soc. Am. A* **11**(7), 1985–1992 (1994).
27. W. T. Welford, "Use of annular apertures to increase focal depth," *J. Opt. Soc. Am.* **50**(8), 749–753 (1960).
28. I. L. Goldberg and A. W. McCulloch, "Annular aperture diffracted energy distribution for an extended source," *Appl. Opt.* **8**(7), 1451–1458 (1969).
29. Z. Wang, A. C. Bovik, H. R. Sheikh, and E. P. Simoncelli, "Image quality assessment: From error visibility to structural similarity," *IEEE Trans. Image Process.* **13**(4), 600–612 (2004).

1. Introduction

In general, the terms lens and imaging have been inseparable, as without lens (or spherical mirror) it is commonly believed that imaging is not possible [1]. However, lensless imaging techniques do exist for many centuries [2–5]. Lensless imaging, besides possessing numerous advantages such as high space-bandwidth product [4], can be a solution to telescopic applications, which generally require large and heavy spherical mirrors, or lenses, whose fabrication requires an enormous amount of material [6]. Synthetic aperture techniques to reduce material in telescope applications involve either the use of many small telescopes sparsely arranged, or the use of segmented mirrors [7,8]. Synthetic aperture based incoherent digital holography techniques demonstrated in the past for super-resolution applications [9–13] also provide a solution to the aforementioned problem. The present study is an attempt to offer an effective alternative to the large and bulky reflective mirrors or refractive/diffractive lenses, commonly used in space, or ground telescopes.

The present research originates from an incoherent digital holography technique known as Fresnel incoherent correlation holography (FINCH) [14]. FINCH works on the principle of self-interference, where both interfering waves carry information of the object, but one of them is modulated by a different quadratic phase mask than the other. Under specific conditions, FINCH exhibits a super lateral resolution beyond the classical limits but has a relatively low axial resolution [15]. Coded aperture correlation holography (COACH) was developed recently based on FINCH by changing the quadratic phase modulation to a pseudorandom phase modulation. COACH shows the same lateral and axial resolutions as of an equivalent incoherent regular imaging system with same numerical aperture [16]. In COACH, the light diffracted by a point object is modulated by a pseudorandom coded phase mask (CPM) and is interfered with the unmodulated version of the light diffracted from the same point object. The resulting impulse response hologram serves as a point spread function (PSF) and is used later as the reconstructing kernel function for all the object holograms. Following the PSF generation, a complicated object is placed at the same axial location of the point object and another hologram, the object hologram, is recorded with the same CPM. The image of the object is reconstructed by a cross-correlation between the PSF and the object hologram. Therefore, for reconstruction of the object corresponding to different depths, a training phase is required in which the point object is shifted to various axial locations and a

library of PSFs are created. The images of the object at different depths are reconstructed by a cross-correlation with the appropriate PSF from the library.

Several interesting and useful properties of COACH such as high axial resolution [16], high spectral resolution [17], and super-resolution capabilities [18] have been unfolding recently. Another stimulating feature of COACH is the fact that 3D imaging can be achieved without two-wave interference [19]. This version of COACH without two-wave interference is termed interferenceless COACH (I-COACH), and it is implemented by an optical configuration as simple as a regular imaging system. The intensity pattern recorded by the I-COACH system can be considered on one hand as a digital hologram generated without interference, but on the other hand, can be treated as an intensity pattern containing the 3D information of the observed scene. The interferenceless property makes I-COACH ideal for numerous applications in which implementing two-wave interference is a difficult task.

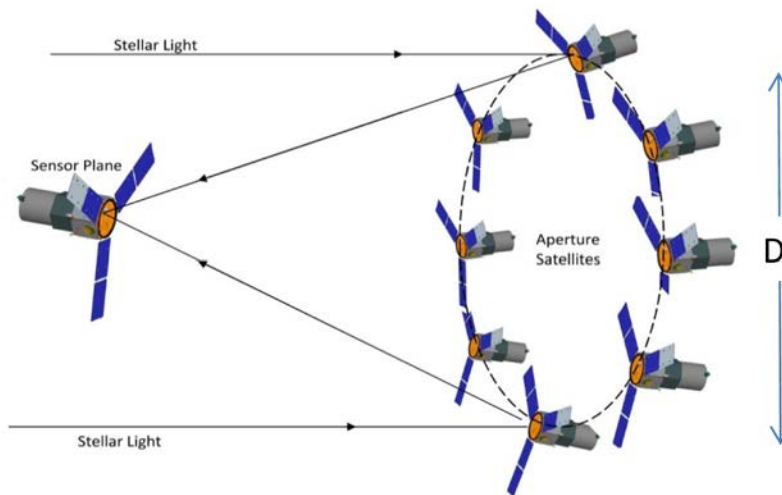


Fig. 1. A scheme for the proposed future space telescope.

In this study, the principle of I-COACH is tested with the concept of a partial aperture imaging system (PAIS). In PAIS, part of the area of the system's clear circular aperture is blocked and consequently, the propagating light is enforced to pass only through the rest of the open area. As is explained in the following, in order to maximize the image resolution, a shape of a ring is chosen as the partial aperture for the present study. We examine how much the aperture area can be reduced and how many images should be captured in order to compensate for the reduction of the effective aperture. In all the previous systems of COACH and I-COACH [16–19,21–23] the images have been captured with a full system aperture. To the best of our knowledge, the present research is the first attempt to acquire images with I-COACH system equipped with a partial aperture.

The vision for a possible application of the present research is illustrated in Fig. 1, in which a possible space telescope is proposed. In this telescope, the system aperture is composed of coded apertures from several spacecraft, distributed along the perimeter of a circle with a diameter D . The goal of such telescope is to yield images of any observed object with as close as possible resolving power and signal-to-noise ratio (SNR) as of a telescope with a complete, clear, continuous aperture with the same diameter D . As a first stage of the research, in this study, we consider the case where the partial aperture has the shape of a continuous ring. Moreover, the imaging system is a table-top miniature optical setup with a spatial light modulator (SLM) used as the system aperture. This setup with the miniature SLM is aimed to be just a proof of the principle. By this principle, it is claimed that a partial aperture of CPM in a shape of a narrow ring can image 3D scene with a comparable

resolution and SNR as of a regular lens-based system with a full aperture of the same diameter. In other words, in this study, we consider whether a partial pseudorandom phase aperture can yield images with a comparable quality as of imaging with a clear circular aperture. In this preliminary stage of the research, the illustration of Fig. 1 is used as a motivation only and is not discussed further in this article.

The manuscript consists of four sections. In the second section, the theoretical analysis of the principle and the methodology are presented. The experiment is discussed in the third section, followed by the conclusion in the last section.

2. Methodology

The operation principles of PAIS and I-COACH with a full aperture [19] are similar, and hence in the following, we briefly summarize these principles. The considered optical system is illuminated incoherently and as so, the system is linear and space invariant for 2D intensity functions from input to output 2D planes. The point spread function of the system is dictated by the system aperture, whereas in [19] and in the present case the pseudorandom CPM is used as the aperture. The goal of the system is to perform indirect 3D imaging. By the term indirect imaging, we mean that any intensity point in the input creates a caustic intensity pattern on the output plane (image sensor), rather than a copy of the point as is in direct imaging. Furthermore, in indirect imaging, the image of the object is usually reconstructed by a computer algorithm. In the present case, the image is reconstructed by the 2D digital correlation between the 2D responses of the system for a multi-point object and for a point on the optical axis. Therefore, before the system can image, it has a period of training in which the response to a point at the origin of the input plane is stored as the reconstructing function. In order to do 3D imaging, one needs to record and store a library of the responses to a point shifted continuously along the Z axis. The training stage is done only once and once it is completed, the imaging stage can start and be applied for an arbitrary number of objects. When the observed scene is 3D, the 2D response to the 3D object is correlated with the entire matrices of the library, whereas each 2D cross-correlation reconstructs a different axial cross-section. The cross-correlation between two caustic functions suffers from a high level of background noise. To minimize the level of the noise we have operated in four different directions. First, the CPM is synthesized by Gerchberg-Saxton algorithm (GSA) [20], whereas the constraint of the algorithm on the sensor plane influences the noise level of the final image. Second, we project the entire positive intensity responses onto the complex domain. The projection is performed by recording three responses with three independent CPMs and superposing them with the appropriate complex constants. There are two reducing noise effects here; the bias terms, one of the main sources of the background noise, are minimized. Additionally, there is an effect of averaging between three statistically independent responses, which reduces the noise as happens with most of the averaging operations in statistics. The third way to increase the SNR is to look on the reconstruction as a pattern recognition problem, in which the goal is to obtain the strongest and the sharpest correlation peak wherever there is point response on the pattern of the object response. Phase-only filter is the spatial filter that yields the desired correlation peak and it is used extensively in our reconstruction process. Finally, if there is still an unaccepted level of noise, the fourth method is executed, in which we average over several complex valued matrices of the reconstruction, each of which is obtained with a different independent set of three CPMs.

The optical configuration of PAIS is shown in Fig. 2. The light from an incoherent source is aimed to illuminate a pinhole used to imitate a point object, and the light diffracted from the object is collimated by a refractive lens L_1 . Lens L_1 is used to emulate an object located far from the imaging system. Therefore, objects close to the front focal plane of lens L_1 can be considered as located in the far field for the CPM, and L_1 can be considered as part of the illumination, rather than of the imaging system. The collimated light is modulated by a pseudorandom CPM limited by a ring of some thickness. The CPM is synthesized using GSA

to render a pure phase function with a limited area on the sensor plane and zero intensity outside this area, as shown in Fig. 3. The light scattered by the CPM is projected on the sensor using an annular diffractive lens to satisfy the Fourier relations of the GSA between the CPM and the sensor planes. If the CPM is removed from the optical configuration, the system becomes a regular imaging system equipped with a partial aperture of an annular diffractive lens, and this latter system is compared with the proposed PAIS in the following. In order to avoid the light outside of the ring from reaching the sensor, a diffractive optical element (DOE) is displayed on the SLM in a shape of a disc with a radius equal to the internal radius of the ring. The DOE is the product of a quadratic phase function with a linear phase function, whereas the linear phase deflects the light, unmodulated by the ring, away from the sensor and the quadratic phase concentrates this unwanted light to a minimal spot size. The DOE enables imitating a system in which only the light passing through the annular CPM arrives at the sensor. The size ratio between the areas of the DOE and CPM can flexibly be changed on the SLM in order to investigate the system under various states of operation and with various annular thicknesses.

Three independent annular CPMs were synthesized by GSA from different initial random phase masks and the corresponding three intensity patterns are recorded similarly to [19]. The recorded intensity patterns are projected onto the complex space with angles $\theta_k = 1,2,3 = 0, 2\pi/3$ and $4\pi/3$ to create a complex matrix considered as the PSF and as the reconstructing matrix. The experiment is repeated by shifting the location of the point object to various axial locations and a library of complex PSFs are created corresponding to the different values of z_s . An object is then placed within the axial boundaries of the PSF library and an object hologram is synthesized from three individual intensity recordings using the same three annular CPMs. The image of the object at different axial locations is reconstructed by a cross-correlation between the object and the PSF recorded at those axial locations.

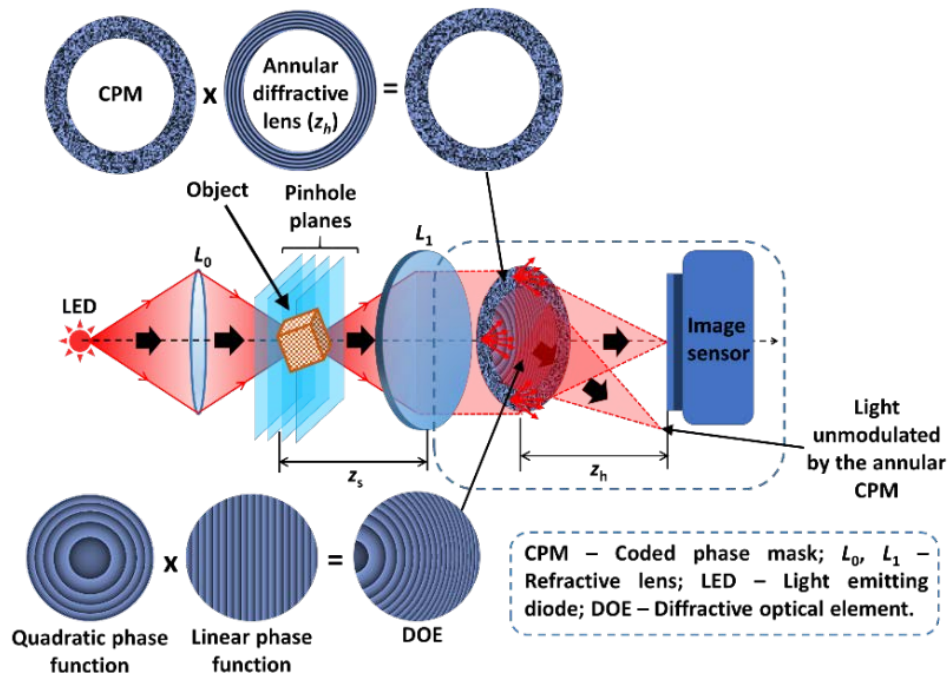


Fig. 2. Optical configuration of PAIS for recording objects and PSFs.

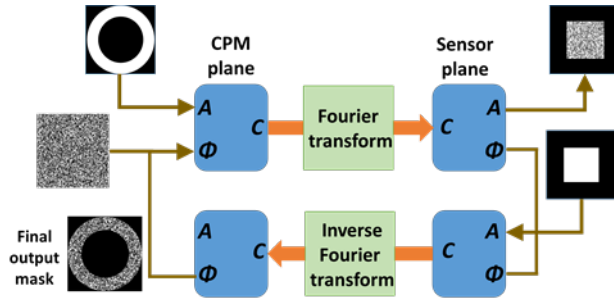


Fig. 3. Schematic of the GSA.

The following analysis is based on the optical configuration given in Fig. 2. Considering a point object located at $(\bar{r}_s, z_s) = (x_s, y_s, z_s)$ with an amplitude $\sqrt{I_s}$, the complex amplitude just before the lens L_1 is given as $\sqrt{I_s} C_0 L(\bar{r}_s/z_s) Q(1/z_s)$, where L and Q represent linear and quadratic phase functions, given by $L(\bar{s}/z) = \exp[i2\pi(\lambda z)^{-1}(s_x x + s_y y)]$ and $Q(a) = \exp[i\pi a \lambda^{-1}(x^2 + y^2)]$ respectively, λ is the wavelength and C_0 is a complex constant. Upon passing through the lens L_1 with a focal length of f_1 , the complex amplitude beyond L_1 is given as $\sqrt{I_s} C_0 L(\bar{r}_s/z_s) Q(1/z_s) Q(-1/f_1)$. Assuming that the distance between L_1 to the CPM is negligible and the diffractive lens is attached to the CPM, the complex amplitude modulated by CPM is given by $\sqrt{\alpha I_s} C_0 L(\bar{r}_s/z_s) Q(1/z_s) Q(-1/f_1) P(\bar{r}) \exp[i\Phi_k(\bar{r})]$, where $\Phi_k(\bar{r})$ is the k -th pseudorandom phase of the annular CPM calculated using the GSA, $P(\bar{r}) [= 1$ for $r_2 \leq |\bar{r}| \leq r_1, = 0$ Otherwise] is a ring function and $\alpha = 1 - (r_1/r_2)^2$ is the fraction of the light intensity modulated by the annular CPM, where r_1 and r_2 are the inner and outer radii of the CPM, respectively. The complex amplitude within the inner radius r_1 , which is not modulated by the CPM is deflected away from the image sensor. The complex amplitude at the image sensor is given as a convolution of $\sqrt{\alpha I_s} C_0 L(\bar{r}_s/z_s) Q(1/z_s) Q(-1/f_1) P(\bar{r}) \exp[i\Phi_k(\bar{r})] Q(-1/z_h)$ with $Q(1/z_h)$. Therefore, the intensity pattern on the image sensor is given by,

$$I_k(\bar{r}_0; \bar{r}_s, z_s) = \left| \sqrt{\alpha I_s} C_0 Q\left(\frac{1}{z_s}\right) L\left(\frac{\bar{r}_s}{z_s}\right) Q\left(-\frac{1}{f_1}\right) P(\bar{r}) \exp[i\Phi_k(\bar{r})] Q\left(-\frac{1}{z_h}\right) * Q\left(\frac{1}{z_h}\right) \right|^2, \quad (1)$$

where the asterisk sign denotes a two-dimensional convolution and $\bar{r}_0 = (u, v)$ is the transverse location vector on the sensor plane. The light diffracted from the CPM is Fourier transformed by the annular diffractive lens of focal length z_h , on the image sensor located at a distance of z_h . Equation (1) can be modified as

$$I_k(\bar{r}_0; \bar{r}_s, z_s) = \left| v \left[\frac{1}{\lambda z_h} \right] \mathfrak{F} \left\{ \sqrt{\alpha I_s} C_0 L\left(\frac{\bar{r}_s}{z_s}\right) Q\left(\frac{1}{z_s}\right) P(\bar{r}) \exp[i\Phi_k(\bar{r})] \right\} \right|^2 \quad (2)$$

$$= I_k \left(\bar{r}_0 - \frac{z_h}{z_s} \bar{r}_s; 0, z_s \right),$$

where $z_1 = z_s f_1 / (f_1 - z_s)$ and v is the scaling operator such that $v[a]f(x) = f(ax)$. The shifting of $I_k(\bar{r}_0; 0, z_s)$ is derived from the shift theorem of the Fourier transform. The second equality of Eq. (2) shows that the intensity on the sensor plane is a shifted version of the intensity response for a point object located on the optical axis ($\bar{r}_s = 0$), where the distance of the shift is $\bar{r}_s z_h / z_s$. The intensity response for object points at the center is used as the k -th component of the PSF.

A 2D object at a distance z_s from the lens L_1 can be considered as a collection of N uncorrelated point objects given by

$$o(\bar{r}_s) = \sum_j^N a_j \delta(\bar{r}_s - \bar{r}_j), \quad (3)$$

where a_j is the intensity of the j -th object point at \bar{r}_j . The object is illuminated by an incoherent quasi-monochromatic light source and therefore there is no interference between the individual point responses, due to the spatial incoherence of the object light. The overall intensity distribution on the sensor plane is a sum of the point responses, given by,

$$I_{OBJ,k}(\bar{r}_0; z_s) = \sum_j a_j I_k\left(\bar{r}_0 - \frac{z_h}{z_s} \bar{r}_j; 0, z_s\right). \quad (4)$$

As $I_{OBJ,k}(\bar{r}_0; z_s)$ and $I_k(\bar{r}_0; z_s)$ are both positive real quasi-random functions, the cross-correlation between them yields an undesired background distribution, mainly because both functions have a dominant bias term. In order to eliminate the bias terms, and consequently, to reduce the background distribution, both $I_{OBJ,k}(\bar{r}_0; z_s)$ and $I_k(\bar{r}_0; z_s)$ are projected onto the complex domain with $\theta_k = 1, 2, 3 = 0, 2\pi/3$ and $4\pi/3$ as follows,

$$H_{PSF}(\bar{r}_0; z_s) = \sum_{k=1}^K I_k(\bar{r}_0; z_s) \exp(i\theta_k), \quad (5)$$

and

$$\begin{aligned} H_{OBJ}(\bar{r}_0; z_s) &= \sum_{k=1}^K I_{OBJ,k}(\bar{r}_0; z_s) \exp(i\theta_k) \\ &= \sum_{k=1}^K \sum_j a_j I_k\left(\bar{r}_0 - \frac{z_h}{z_s} \bar{r}_j; 0, z_s\right) \exp(i\theta_k) \\ &= \sum_j a_j H_{PSF}\left(\bar{r}_0 - \frac{z_h}{z_s} \bar{r}_j; z_s\right), \end{aligned} \quad (6)$$

where $H_{PSF}(\bar{r}_0; z_s)$ and $H_{OBJ}(\bar{r}_0; z_s)$ are the complex PSF and the object holograms, respectively. The number of projections is selected as $K = 3$ in order to have better suppression of the background distribution [17], although it is well-known that in order to eliminate the bias terms $K = 2$ is sufficient (I-COACH with $K = 2$ is described in [21,22]). The image is reconstructed by correlating $H_{OBJ}(\bar{r}_0; z_s)$ with phase-only filtered of $H_{PSF}(\bar{r}_0; z_s)$ given by $\tilde{H}_{PSF}(\bar{r}) = \mathfrak{F}^{-1}\left\{\exp\left[i \cdot \arg\left(\mathfrak{F}\{H_{PSF}(\bar{r})\}\right)\right]\right\}$, in order to reduce the background noise [23]. The image reconstruction can be expressed as follows,

$$\begin{aligned}
O_R(\bar{r}_R) &= \iint H_{OBJ}(\bar{r}_0; z_s) \tilde{H}_{PSF}^*(\bar{r}_0 - \bar{r}_R; z_s) d\bar{r}_0 \\
&= \iint \sum_j a_j H_{PSF} \left(\bar{r}_0 - \frac{z_h}{z_s} \bar{r}_j; z_s \right) \tilde{H}_{PSF}^*(\bar{r}_0 - \bar{r}_R; z_s) d\bar{r}_0 \\
&= \sum_j a_j \Lambda \left(\bar{r}_R - \frac{z_h}{z_s} \bar{r}_j \right) \approx o \left(\frac{\bar{r}_s}{M_T} \right).
\end{aligned} \tag{7}$$

where Λ is a δ -like function, approximately equal to 1 at (0,0) and to small negligible values elsewhere.

During the cross-correlation between the object hologram and the PSF, the dominant reconstructed images are the objects located at the same axial plane of the point creating the PSF. Therefore, in order to extract the complete 3D information of the object, a library of PSF is necessary at all the axial locations corresponding to the depth of the object. The reconstructed image obtained from Eq. (7), is a magnified image of the object, with a transverse magnification of $M_T = z_h/z_s$. Since the image is reconstructed using correlation, the transverse and axial resolutions are governed by the transverse and axial correlation lengths, determined by the size of the smallest spot that can be recorded on the sensor plane by the SLM with an active area of diameter of D . Among all the partial apertures limited by a disc of diameter D , the aperture of a ring with an outer diameter of D yields the smallest spot on the sensor plane. The goal to achieve maximum lateral resolution is the reason for choosing the annular aperture. Therefore, PAIS is expected to exhibit similar lateral and axial resolutions of I-COACH with the same numerical aperture (NA).

A regular imaging system with an annular aperture can be considered in the same optical configuration, in the absence of the CPM. The intensity at the image sensor for a point object located at (\bar{r}_s, z_s) is given as,

$$I_{RI}(\bar{r}_0; \bar{r}_s, z_s) = \left| v \left[\frac{1}{\lambda z_h} \right] \mathfrak{F} \left\{ \sqrt{\alpha I_s} C_0 L \left(\frac{\bar{r}_s}{z_s} \right) \mathcal{Q} \left(\frac{1}{z_1} \right) P(\bar{r}) \right\} \right|^2. \tag{8}$$

The imaging of objects using an annular lens has been studied and found to have an enhanced lateral resolution [24–27]. As the thickness of the annular ring decreases, the central peak narrows while the height of the PSF sidelobes increases resulting in a redistribution of light from the central peak to the side lobes [28]. Therefore, at some limiting value ($\alpha \ll 1$), the signal cannot be retrieved. However, in the case of PAIS, the imaging is indirect and hence the sidelobes are lower. Moreover, with averaging over many complex reconstructions, the caustic side-lobe distribution is reduced toward zero mean, and hence the image of the object can be retrieved with improved SNR.

3. Experiments

The experimental study of PAIS is carried out using the setup shown schematically in Fig. 4. The photograph of the experimental setup is shown in Fig. 5. The setup consists of two illumination channels with identical light emitting diodes (LEDs) (Thorlabs LED635L, 170 mW, central wave length of $\lambda = 635$ nm, full width at half maximum $\Delta\lambda = 15$ nm) critically illuminating by identical lenses L_{0A} and L_{0B} two resolution targets, negative National Bureau of Standards charts (NBS) (NBS 1963A Thorlabs). Initially, a pinhole with a diameter of 25 μm is mounted at a distance of 3 cm from the lens L_{0A} and the LED2 is turned off. The light diffracted by the pinhole is incident on a beam splitter BS_1 and collimated by a lens L_1 with a diameter of 2.5 cm and a focal length $f_0 = 20$ cm resulting in an NA of ~ 0.06 . A polarizer P is used to allow only the light oriented along the active axis of the SLM (Holoeye PLUTO, 1920 \times 1080 pixels, 8 μm pixel pitch, phase-only modulation) located at a distance of around 10 cm from the lens L_1 . On the SLM, a phase mask containing the CPM synthesized using GSA and

an annular diffractive lens, both with same inner and outer radii r_1 and r_2 are displayed. Three CPMs synthesized from different initial random phase profiles are displayed and the corresponding intensity patterns are recorded at the image sensor (Hamamatsu ORCA-Flash4.0 V2 Digital CMOS, 2048×2048 pixels, $6.5 \mu\text{m}$ pixel pitch, monochrome) which is located at a distance of approximately 25 cm from the SLM. The specifications of the computer used are as follows: 32 GB RAM and the processor of Intel(R) i7-5930K, CPU @ 3.50 GHz.

The three intensity patterns are superposed according to Eq. (5) to yield the PSF. The experiment is repeated for different values of $r_1 = 0, 3.92 \text{ mm}, 4.16 \text{ mm}, 4.24 \text{ mm}$ and 4.28 mm while r_2 is maintained at 4.32 mm resulting in approximate aperture area ratios of 0.785, 0.14, 0.06, 0.03 and 0.014 respectively.

In the first experiment, an NBS resolution target with 14 lp/mm is mounted in channel 1 and a pinhole is mounted in channel 2. The two objects were mounted on the same axial location and the pinhole and object responses were recorded using the same CPMs for the different ratios between the inner and outer radii. The image of the object is reconstructed by a cross-correlation between the object and the phase-only filtered (POF) version of the PSF [23]. The reconstruction is further improved by blocking the noise by a low-pass filter with the area of about 3% of the entire Fourier domain. The three intensity patterns recorded for the pinhole and for the object, with three independent CPMs, are shown in the first three left-hand columns of Fig. 6. In the next two columns the magnitude and phase of the complex PSF, and of the object holograms, are shown. The image reconstructions for the different areas of the aperture in the case of PAIS, and of regular imaging, are shown in the most right-hand column of Fig. 6. It can be noted that when the width of the ring aperture decreases from the full circular aperture to $400 \mu\text{m}, 160 \mu\text{m}, 80 \mu\text{m}$ and $40 \mu\text{m}$, the reconstructed images deteriorated. However, the contrast of the images of PAIS is always better than those of the regular annular system.

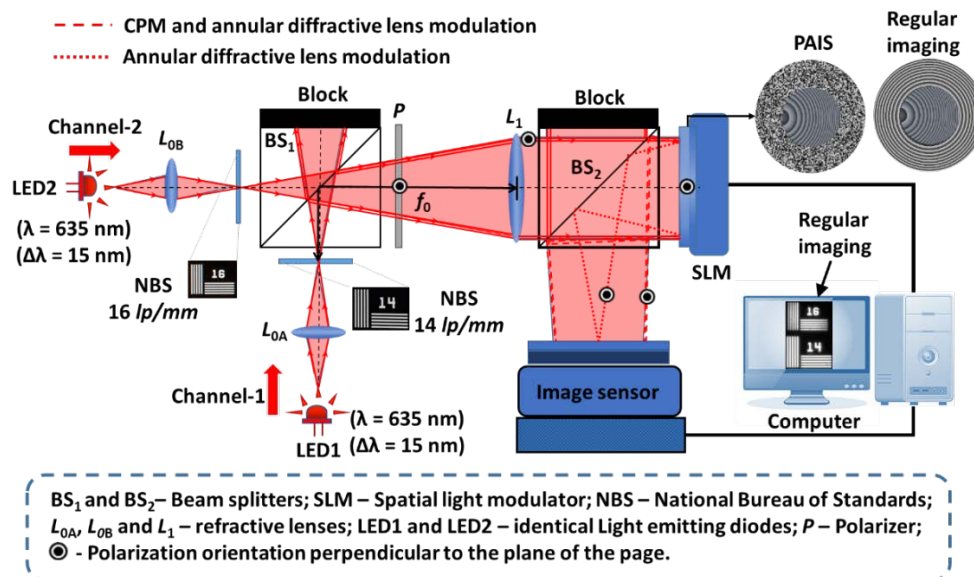


Fig. 4. Experimental setup of PAIS with two illumination channels.

The next experiment is aimed to test the influence of averaging over several image reconstructions. In this experiment, the pinhole is replaced by another NBS object 16 lp/mm in channel 2. The two NBS objects are spatially separated to assure that there is no interference between the light diffracted from them. The object holograms were recorded when object 14 lp/mm and object 16 lp/mm are located at 20 cm from the lens L_1 . The images

of the objects were reconstructed by a cross-correlation between the object hologram and the same low-pass filtered, POF version of the PSF. An averaging technique is implemented which involves recording intensity patterns with different sets of CPM synthesized by GSA from different random phase profiles and averaging the complex reconstructions. In this case, 21 sets of three CPMs were created and the corresponding intensity patterns were recorded for the PSF and the object holograms and the resulting complex reconstructions were averaged. The averaged reconstructions for different ring widths are compared with regular imaging with the annular diffractive lens of the same ring widths as shown in Fig. 7. We conclude that besides the case of full aperture, in all other cases the quality of the reconstructed images from PAIS is superior over the images from the regular imaging.

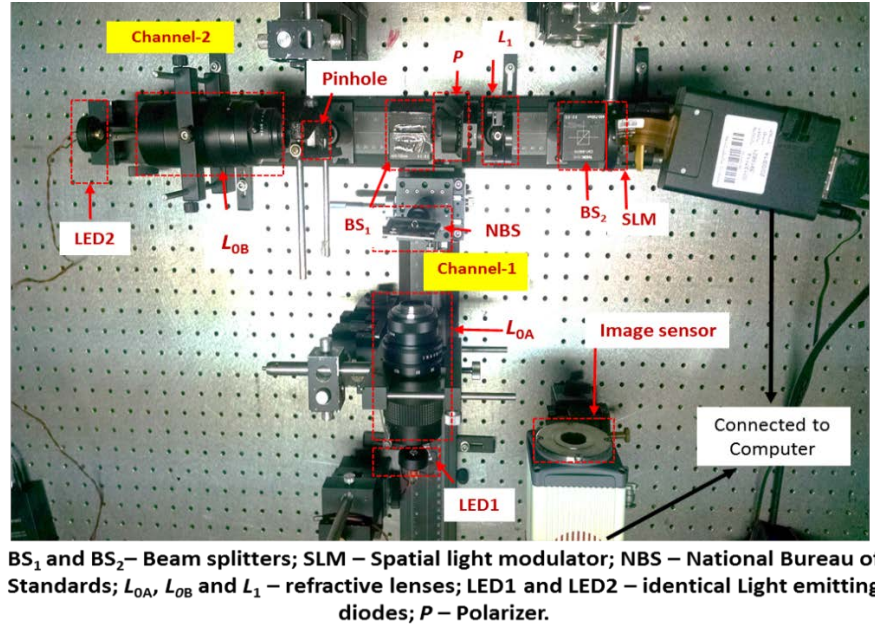


Fig. 5. Photograph of the experimental setup of PAIS.

Next, the mean squared error (*MSE*) is calculated versus the number of reconstructed CPM sets in the PAIS. *MSE* is calculated as,

$$MSE = \frac{1}{MN} \sum_{m=1}^M \sum_{n=1}^N |O_{RI}(m,n) - \gamma O_R(m,n)|^2, \quad (9)$$

where O_{RI} and O_R are $M \times N$ matrices of the desired and obtained reconstruction of the object, respectively. A reconstruction close to regular imaging with full aperture is desirable and hence O_{RI} is the image of the object recorded by regular imaging with full aperture and

$$\gamma = \frac{\sum_{m=1}^M \sum_{n=1}^N O_{RI}(m,n) O_R(m,n)}{\sum_{m=1}^M \sum_{n=1}^N |O_R(m,n)|^2} \quad (10)$$

The plots of *MSE* versus CPM sets, for different values of annular width, are shown in Fig. 8. By averaging over the independent reconstructions, the *MSE* decreases, but beyond a particular number of CPM sets, it reaches an almost constant value.

The structural similarity (*SSIM*) between an ideal image obtained by regular imaging using the full aperture and the results of regular imaging and PAIS with different annular aperture thickness are calculated [29] as

$$SSIM(I_1, I_2) = \frac{(2\mu_{I_1}\mu_{I_2} + C_1)(2\sigma_{I_1I_2} + C_2)}{(\mu_{I_1}^2 + \mu_{I_2}^2 + C_1)(\sigma_{I_1}^2 + \sigma_{I_2}^2 + C_2)}, \quad (11)$$

where, I_1 and I_2 are the two images compared; μ_{I_1}, μ_{I_2} are the local mean values of the images I_1 and I_2 ; $\sigma_{I_1}, \sigma_{I_2}$ are the variances of images I_1 and I_2 ; $\sigma_{I_1I_2}$ is the covariance; C_1 and C_2 are constants used to avoid instability when the sum of squares of local mean or variance becomes close to zero in the denominator. *SSIM* index is considered as a reliable tool to estimate the quality of degraded images in comparison to a reference image [29]. The *SSIM* index maps are shown in Fig. 9, where brightness indicates the magnitude of the local *SSIM* index. The plot of the mean *SSIM* values is shown in Fig. 10, from which the superiority of PAIS over the regular imaging is clearly verified quantitatively.

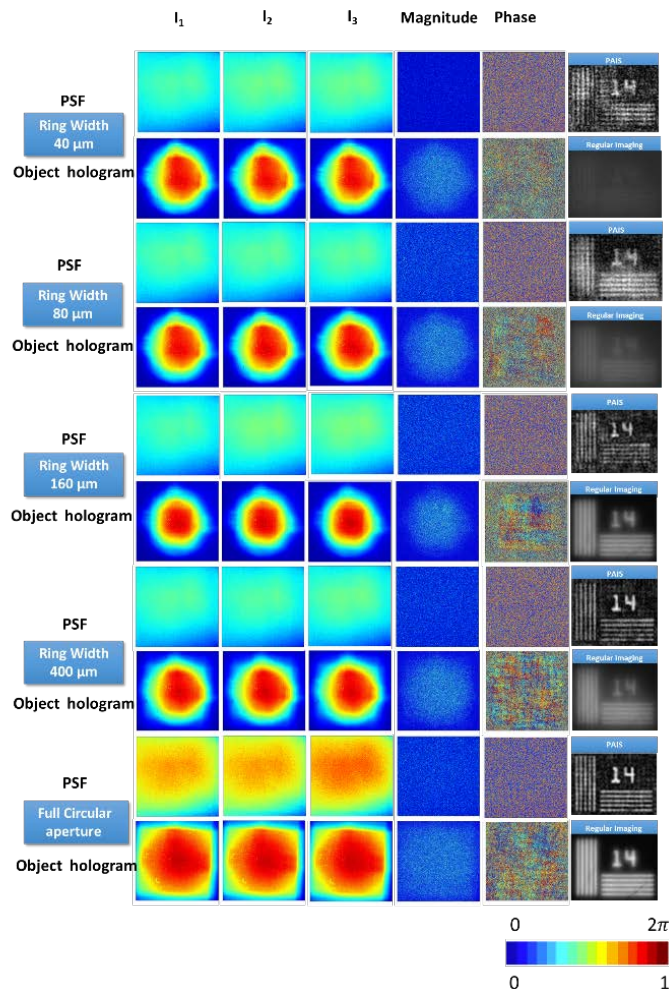


Fig. 6. Intensity patterns, magnitude and phase of the complex holograms for the pinhole and the object, their reconstructions and regular imaging for ring widths 40 μm , 80 μm , 160 μm , 400 μm and 4.3 mm (full aperture).

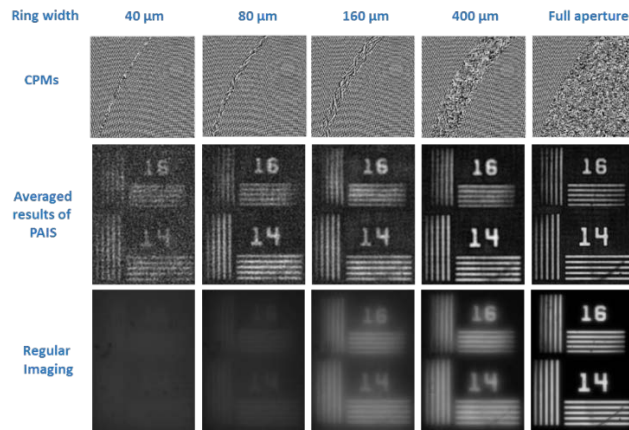


Fig. 7. Top line: part of phase masks with CPMs displayed on the SLM. Middle line: the averaged reconstruction results of PAIS with 21 independent reconstructions. Lower line: regular imaging results for ring widths 40 μm, 80 μm, 160 μm, 400 μm and full aperture when the two resolution charts are placed at the same axial location.

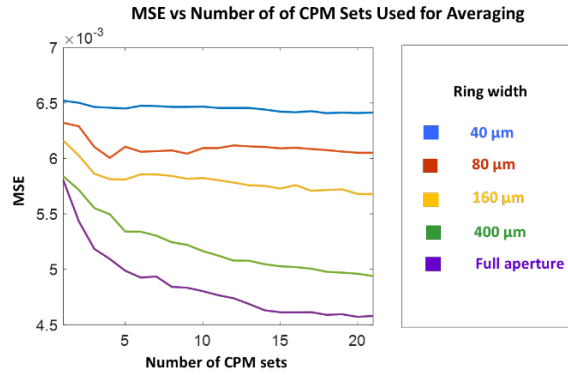


Fig. 8. Plot of the *MSE* of averaged reconstruction results (21 CPM sets) of PAIS for various ring widths.

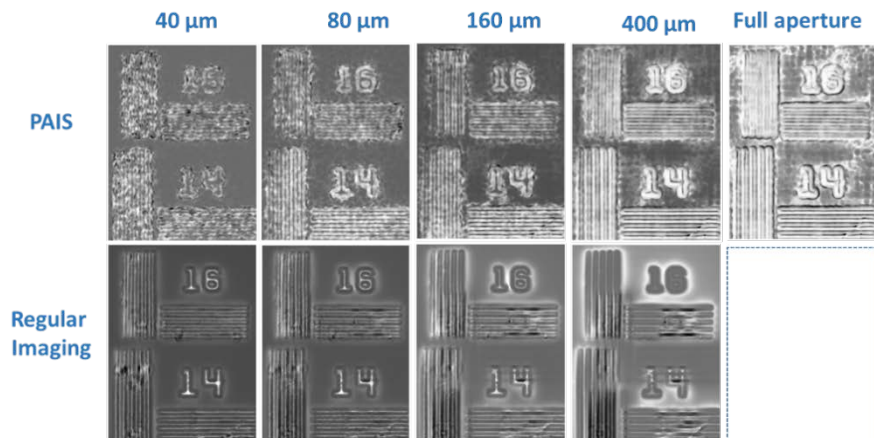


Fig. 9. Top line: *SSIM* index maps of the averaged reconstruction results of PAIS with 21 independent reconstructions. Lower line: *SSIM* index maps of regular imaging results for ring widths 40 μm, 80 μm, 160 μm, 400 μm and full aperture when the two resolution charts are placed at the same axial location while considering full aperture regular imaging as reference image.

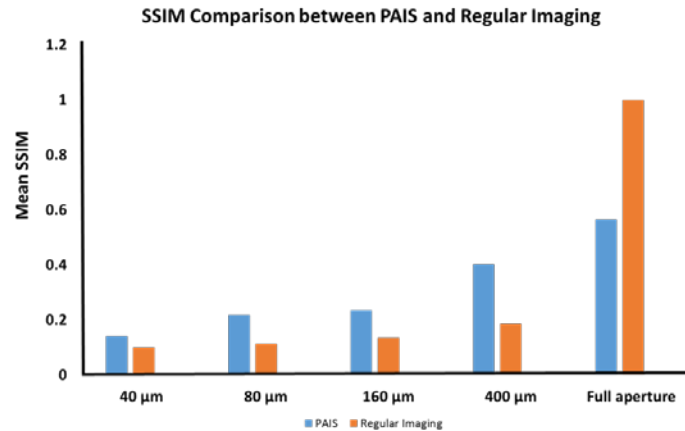


Fig. 10. Plot of the mean SSIM values for PAIS and regular imaging for ring widths 40 μm, 80 μm, 160 μm, 400 μm and full aperture.

Visibility of a grating image [i.e. $(I_{\max} - I_{\min}) / (I_{\max} + I_{\min})$] can be used as an indication of the resolving power of an imaging system [12]. Figure 11 shows the visibility plots of the gratings of the averaged reconstructed images of PAIS and regular imaging for ring widths of 40 μm, 80 μm, 160 μm and 400 μm. PAIS exhibits high visibility consistently for all the ring widths while regular imaging shows poorer visibility. As is shown in Fig. 6, and quantitatively in Fig. 11, the performances of regular imaging decreases with the reduction of the ring thickness, whereas the reconstruction results of PAIS shows almost the same high contrast and visibility for all the annular width values.

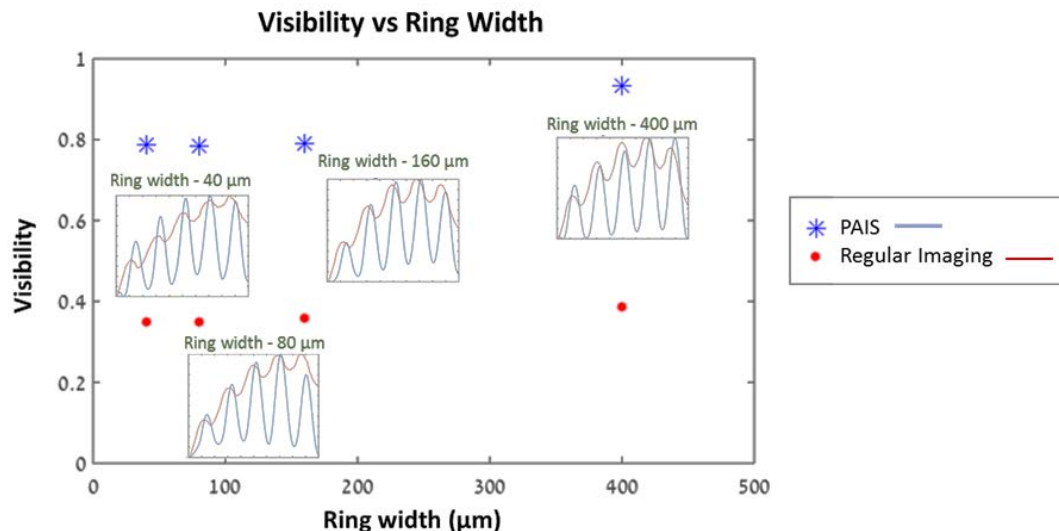


Fig. 11. Plot of the visibility of the gratings on the resolution chart for regular imaging and PAIS for ring widths of 40 μm, 80 μm, 160 μm and 400 μm.

The next experiment is carried out to study the 3D imaging capabilities of PAIS. The NBS object of 16 lp/mm in channel 2 is replaced by the pinhole translated to a new axial location far away by 1 cm from the previous location. The PSFs are recorded for 17 sets of CPMs with different ring widths. The pinhole is then replaced by the NBS object of 16 lp/mm located at the new axial location. The intensity patterns are recorded for the two-plane object and composed into a complex hologram for the same 17 sets of CPMs for different ring widths.

The object holograms are correlated with PSFs recorded at two different axial locations and the resulting complex reconstructions were averaged over the 17 reconstructions. The experiment is repeated for regular imaging by changing the focal length (27.3 cm) of the annular diffractive lens such that the new axial plane is in focus. The comparison results of PAIS and regular imaging are shown in Fig. 12. Once again, the averaged reconstructions result retrieved the 3D information while regular imaging failed for smaller areas of the aperture.

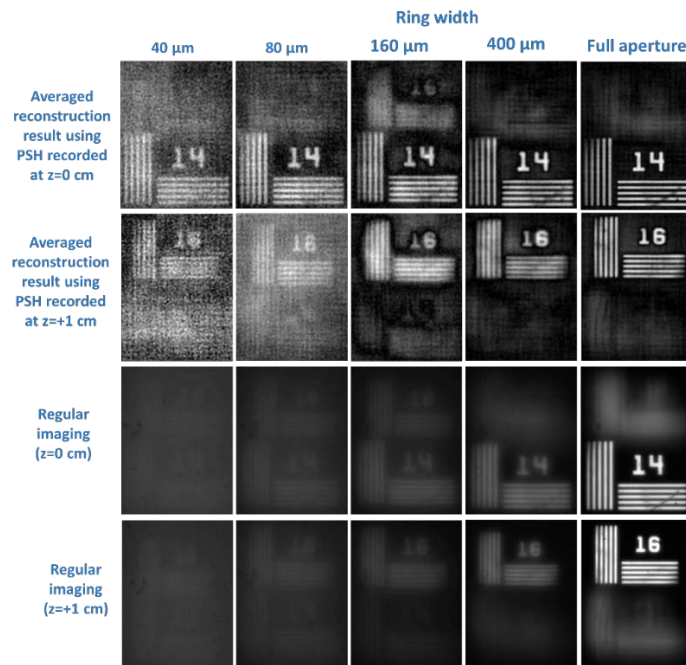


Fig. 12. Comparison of the averaged reconstruction results of PAIS with 17 samples and regular imaging results for ring widths 40 μm, 80 μm, 160 μm, 400 μm and full aperture when the two objects are separated by a distance of 1 cm.

4. Summary and conclusions

We have studied the capabilities of partial aperture imaging of PAIS by designing annular CPMs with areas of a relatively small fraction of the total areas of the aperture. In PAIS, the light diffracted from a point object is modulated by a CPM and it is projected on the sensor plane using an annular diffractive lens with the same aperture specifications. The resulting intensity responses are recorded and superposed as a complex PSF. An object is then placed at the same axial location of the point object and the object hologram is recorded using the same CPM. The image of the object is reconstructed by a cross-correlation between the above two holograms. For reconstruction of a 3D object, a library of PSFs are recorded corresponding to the different axial locations. The image of the object at any axial plane is reconstructed by a cross-correlation between the object hologram and the PSF recorded at the same axial location.

The experiment is repeated by reducing the area of the CPM and the results were compared with that of regular imaging. The performance of regular imaging was steadily deteriorated with the decrease in the aperture area until the image could not be recognized. On the other hand, the reconstruction results of PAIS were recognizable until the narrowest aperture ring, although the amount of distortions is increased with the aperture reduction. The MSE of the reconstruction was reduced using the averaging technique with CPMs synthesized from different initial random phases. PAIS demonstrated 3D imaging capability with an

aperture area of as low as 1.4% of the total area of the aperture while regular imaging can yield an identifiable image with an aperture area of no less than 6%.

The collimating lens L_1 in the experimental setup of PAIS can be removed for far-field imaging as the sections of the wavefronts encountering the area of the CPM from long distances are almost parallel. The annular diffractive lens can be integrated into the CPM using modulo- 2π phase addition technique as it is shown in the experiment, and therefore PAIS can be considered as a lensless imaging technique. The experimental procedure seems to consume a lot of time. However, it must be noted that the recording of the PSH libraries is done only once as part of training the system. Furthermore, the image capture can be automated when object holograms for different CPMs were recorded resulting in a reduced imaging time of few minutes with PAIS. The superior imaging capabilities of PAIS make it a serious candidate for future ground-based and spacecraft telescopes.

Funding

Israel Science Foundation (ISF) (Grants No. 1669/16); Israel Ministry of Science and Technology (MOST).